The American Journal of Pathology, Vol. 178, No. 2, February 2011

DOI: 10.1016/j.ajpath.2010.10.019

Cell Injury, Repair, Aging, and Apoptosis

A Quantitative Approach to Scar Analysis

Hooman Khorasani,* Zhong Zheng,† Calvin Nguyen,‡ Janette Zara,§ Xinli Zhang,† Joyce Wang,¶ Kang Ting,†‡§ and Chia Soo†

From the Division of Dermatologic & Cosmetic Surgery, The Mount Sinai Medical Center, New York, New York; the Department of Orthopaedic Surgery,† David Geffen School of Medicine, the School of Dentistry,‡ and the Department of Bioengineering,§ University of California, Los Angeles, Los Angeles, California; and the School of Medicine,¶ University at Buffalo, Buffalo, New York*

Analysis of collagen architecture is essential to wound healing research. However, to date no consistent methodologies exist for quantitatively assessing dermal collagen architecture in scars. In this study, we developed a standardized approach for quantitative analysis of scar collagen morphology by confocal microscopy using fractal dimension and lacunarity analysis. Full-thickness wounds were created on adult mice, closed by primary intention, and harvested at 14 days after wounding for morphometrics and standard Fourier transform-based scar analysis as well as fractal dimension and lacunarity analysis. In addition, transmission electron microscopy was used to evaluate collagen ultrastructure. We demonstrated that fractal dimension and lacunarity analysis were superior to Fourier transform analysis in discriminating scar versus unwounded tissue in a wild-type mouse model. To fully test the robustness of this scar analysis approach, a fibromodulin-null mouse model that heals with increased scar was also used. Fractal dimension and lacunarity analysis effectively discriminated unwounded fibromodulin-null versus wild-type skin as well as healing fibromodulin-null versus wild-type wounds, whereas Fourier transform analysis failed to do so. Furthermore, fractal dimension and lacunarity data also correlated well with transmission electron microscopy collagen ultrastructure analysis, adding to their validity. These results demonstrate that fractal dimension and lacunarity are more sensitive than Fourier transform analysis for quantification of scar morphology. ***(Am J Pathol 2011, 178:621–628; DOI: 10.1016/j.ajpath.2010.10.019)***

Cutaneous scarring can lead to major cosmetic, psychological, and functional consequences in patients with hypertrophic scars from burn injuries or keloid scars. To gain further insight into scar formation, it is essential to be able to better correlate the molecular events during wound repair with changes in collagen architecture. Because 85% of the dermis consists of collagen,[1] dermal elasticity and strength are primarily determined by collagen with lesser contributions from elastin and other extracellular matrix constituents.[2,3] At present, no consistent methodologies exist for quantitatively assessing dermal collagen architecture. Despite the integral nature of collagen ultrastructure and architecture to wound healing research, few studies have been conducted on evaluation of collagen architecture, with most studies published decades ago.[4]

Qualitative histopathologic studies of cutaneous scar tissue show more tightly packed collagen bundles with orientations parallel to the epidermis rather than the loose, random, basket-weave–like organization of collagen bundles in normal dermis.[5] Currently traditional scar morphology and collagen architectural analyses are performed by one or two observers, using conventional light microscopy in combination with polarized light.[6,7] More objective methods such as X-ray diffraction,[8,9] laser scattering,[10,11] and Fourier transform analysis[3,4,12] also have been recently described. Head-to-head comparisons of these modalities indicate that Fourier transform analysis, which provides information about collagen bundle orientation, randomness, and spacing,[12] appears to be the superior method. However, Fourier transform analysis has limitations when applied to analysis of complex biological structures at high magnification. The primary aim of this study is to demon-

Supported by National Institutes of Health grant R21 DE015118-01; by the Wunderman Family Foundation; and by the Plastic Surgery Research Foundation.

Accepted for publication October 13, 2010.

C.S. and K.T. are inventors of fibromodulin-related patents.

Supplemental material for this article can be found at *http://ajp.amjpathol.org* and at doi:10.1016/j.ajpath.2010.10.019.

Address reprint requests to Chia Soo, M.D., FACS, Department of Orthopaedic Surgery, University of California at Los Angeles, MRL Rm 2641A, 675 Charles E Young Dr South, Los Angeles, CA 90095-1759. E-mail: bsoo@ucla.edu. Or Kang Ting, DMD, DMSc, School of Dentistry, University of California at Los Angeles, CHS 30-117, 10833 Le Conte Ave, Los Angeles, CA 90095. E-mail: kting@dentistry.ucla.edu.

strate a new objective and quantitative approach to collagen morphology analysis that is more robust than Fourier transform analysis and can be used for analysis of complex biological structures.

In this study, we demonstrate analysis of scar collagen morphology using the concepts of fractal dimension (F_D) and lacunarity (L). F_D provides a measure of how completely an object fills space and increases in value with increasing structural density.[13] It has a value between 1 and 2: a minimum value of 1 corresponds to a straight line filling the space, and a maximum value of 2 corresponds to an object completely occupying the entire space. However, F_D alone is not sufficient to discriminate completely between objects because different fractal sets may have the same F_D value and yet have strikingly different textures. Therefore Mandelbrot introduced the term *lacunarity* to describe the characteristics of fractals of the same dimension with different texture appearances.[14] L is a measure of the nonuniformity (heterogeneity) of a structure or the degree of structural variance within an object.[13] Simplistically, low L objects are homogeneous, whereas high L objects are heterogeneous. L has a value between 0 and 1, where a minimum value of 0 corresponds to an absolute homogeneous object. F_D and L have previously exhibited accuracy and reproducibility when applied to complex biological structures such as neurons,[15] alveoli,[16] and capillary beds.[17] However, to our knowledge this is the first application of F_D and L concepts to dermal scar investigation.

To fully test the robustness and sensitivity of applying F_D and L analysis to dermal architecture, we tested not only unwounded skin (relatively quiescent deposition/collagen remodeling) versus wounded skin (active collagen deposition/remodeling) in normal wild-type (WT) mice but also 2-week wounds from WT mice versus fibromodulin (FMOD)-null ($FMOD^{-/-}$) mice (active collagen deposition/remodeling in two different genetic backgrounds), as well as unwounded skin from WT and $FMOD^{-/-}$ mice. FMOD is a member of the small leucine-rich proteoglycan family[18] with important roles in collagen fibrillogenesis, ultrastructure, and histologic architecture.[19–23] Our secondary goal was to determine whether F_D and L analysis could finely discriminate genotypic differences in collagen architecture under complicated, acute wound healing conditions. In addition, to determine whether F_D and L data correlate with collagen ultrastructure, we also performed transmission electron microscopy (TEM) on unwounded and wounded skin from WT and $FMOD^{-/-}$ mice.

Lastly, much like scar morphology, an objective standardized approach for evaluation of scar size has yet to be established, and histopathological analysis remains the gold standard for evaluation of scar size. Because cutaneous scarring is essentially defined by dermal rather than epidermal scar tissue, variable dermal thickness due to influence of animal age, sex, genotype, or scar age can affect scar size measurements. We demonstrate here a new objective method for determining scar size by light microscopy: the scar area (A) is divided by the average dermal thickness (T_{avg}) to obtain a single numerical value (A/T_{avg}) that can be compared among animals with variable dermal thickness.

Materials and Methods

Animal Surgical Procedure and Tissue Preparation

All experiments were performed under institutionally approved protocols provided by the Chancellor's Animal Research Committee at the University of California, Los Angeles, and the Institutional Animal Care and Use Committee at the University of Southern California. $FMOD^{-/-}$ mice were provided by our collaborator Dr. Åde Oldberg (Lund University, Sweden) and genotyped. Male and female WT and $FMOD^{-/-}$ mice (~30 g) ages 3 to 6 months were anesthetized, and the dorsal skin was sterilely prepared. Four full-thickness, 10 mm × 3 mm skin ellipses with the underlying panniculus carnosus muscle were excised on each mouse and closed primarily with 4−0 nylon using two simple interrupted sutures consistently placed at one-third intervals in each 10-mm–length wound. To minimize regional cephalocaudal and dorsoventral differences in wound healing, spatial landmarks such as the forelimb and hind limb articulation sites and the spine were used to consistently mark wound locations. All wounds were separated by at least 2 cm to minimize adjacent wound effects. Wounds were harvested at 2, 7, and 14 days after injury. Unwounded skin from identical locations of WT and $FMOD^{-/-}$ animals were collected as controls. Tissue samples for histology were bisected centrally between the two 4−0 nylon sutures and perpendicular to the long axis of each 10-mm–length wound and fixed in 10% formalin. After fixation, the samples were dehydrated, paraffin-embedded, and cut into either 5-μm sections for H&E staining or 7-μm sections for picro Sirius red staining. To ensure consistent sampling from the center rather than the periphery of the wound, sections were obtained from the cut surface of the wound where it was previously bisected.

Optical Microscopy

H&E staining photographs were captured on an Olympus BX51 microscope (Olympus America Inc., Center Valley, PA) equipped with MicroFire 2.2 digital camera (Optronics, Goleta, CA) using PictureFrame 2.0 software (Optronics) at 40× magnification. Image analysis was performed using the NIH program ImageJ, available as shareware from the NIH website (*http://rsbweb.nih.gov/ij/*).

The influence of animal age, sex, genotype, and scar age on dermal thickness was investigated to prevent possible confounding factors in the scar size analysis. Dermal thickness was defined as the distance from the epidermal-dermal junction down to the panniculus carnosus visualized by H&E stain. Using ImageJ, dermal thickness measurements were obtained on 40× light microscope images by drawing a line normal to the average orientation of the epidermal-dermal and dermal-subcutaneous tissue demarcations. Four dermal thickness mea-

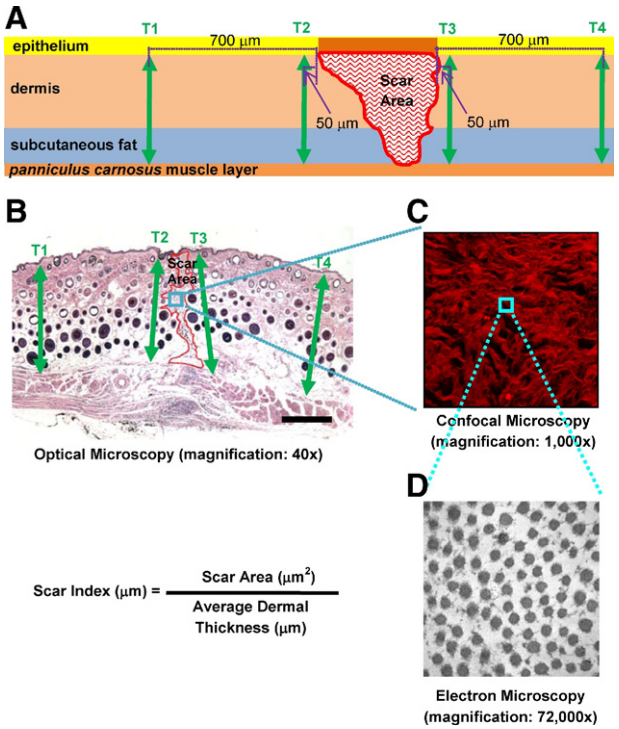

Figure 1. Schematic (**A**) and corresponding H&E image (**B**) illustrating the measurements used for scar size analysis. The wound region used for confocal microscopy (**C**) and transmission electron microscopy (**D**) images and the respective objectives used are shown. Using ImageJ, scar thickness measurements were obtained by drawing a line roughly perpendicular to the average orientation of the epidermal/dermal and panniculus carnosus tissue demarcations. Four dermal thickness measurements were taken per sample (**arrows**)—two adjacent to the wound site at 50 μm away from the left and right wound edges (T2 and T3) and two at 700 μm away from the left and right wound edges (T1 and T4). To obtain scar size, fibrotic scar tissue area (**A**) was outlined using the freeform outline tool in ImageJ and was measured to extend from the base of the epidermis to the panniculus carnosus. Scar size was determined by the Scar Index, calculated by dividing the scar area by the corresponding average dermal thickness: Scar Index (μm)=Scar Area (μm^2)/Average Dermal Thickness (μm).

surements were taken per sample—two adjacent to the wound site at 50 μm on either side, and two at a farther distance of 700 μm on either side of the wound (Figure 1, A and B).

Scar area analysis was performed on H&E staining photographs from WT and FMOD$^{-/-}$ 14-day postoperative wounds in 5- to 6-month-old male mice. Fibrotic scar tissue was outlined using the freeform outline tool in ImageJ to produce a pixel-based area measurement that could then be converted to square micrometers. Like the dermal thickness measurements, scar area measurements were performed extended to the panniculus carnosus (Figure 1, A and B). A positive and predictive relationship was established between dermal thickness and scar area. Scar size is determined by the Scar Index, which is calculated by dividing the scar area (A, in μm^2) by the corresponding average dermal thickness (T_{avg}, in μm); Scar Index = A/T_{avg} (Figure 1, A and B).

Confocal Laser Scanning Microscopy

For analysis of collagen architecture, 14-day postoperative wounds of 5- to 6-month-old WT and FMOD$^{-/-}$ male mice were stained using the modified picro Sirius red technique. After identification by optical microscopy, confocal photographs were captured by a Leica TCS-SPMP confocal microscope (Leica Imaging Systems LTD, Cambridge, UK) at 1000× magnification.[24] Sections were scanned in 1-μm increments for the entire section thickness of 7 μm. Data of frame-mode images were recorded and stored as 512 × 512 pixel images (Figure 1C).

To illustrate the complexity and organization of collagen fibers in quantitative terms, the two-dimensional discrete Fourier transform statistical analyses on all images were processed using a Matlab routine (The MathWorks, Inc., Natick, MA). Briefly, for a confocal image containing a set of aligned collagen fibers, the intensity plot of the corresponding two-dimensional discrete Fourier transform image is expected to have an elliptical pattern. In contrast, for an image with randomly oriented fibers, the intensity plot of the corresponding two-dimensional discrete Fourier transform image should show a circular pattern. The anisotropy of the image is defined by the aspect ratio, which ranges from 0 to 1. A sample is more anisotropic if the aspect ratio is close to 0, whereas it is more isotropic when the aspect ratio is closer to 1.

F_D and L analyses also were performed on the confocal images by using the Frac_Lac add-on to ImageJ (*http://rsbweb.nih.gov/ij/plugins/fraclac/fraclac.html*). For each sample, three middle sections were chosen to capture dimensionality for the analysis. Colored images were first converted to gray scale and subsequently to binary images. Finally, collagen fibers were outlined and ana-

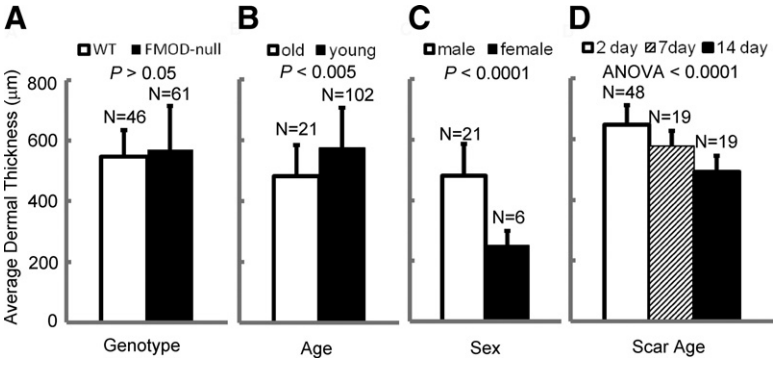

Figure 2. The influence of genotype (**A**), age (**B**), sex (**C**), and scar age (**D**) on average dermal thickness in mice. No significant difference in dermal thickness was found between FMOD-null and WT animals (**A**); 3- to 4-month-old mice had significantly thicker dermis than did 5- to 6-month-old mice (**B**); male mice also had significantly thicker dermis compared with age-matched female mice (**C**); and dermal thickness decreased with increasing scar age in both FMOD-null and WT animals (**D**). ANOVA indicates analysis of variance.

lyzed. A slow-scan, autothreshold sliding-box method was used from minimum box size of one pixel to maximum size of 45% of the region of interest.

TEM

For ultrastructural analysis of collagen architecture, wounded and unwounded skin were fixed in 3% glutaraldehyde in 25 mmol/L sodium acetate, pH 5.7, 0.3 M $MgCl_2$, and 0.05% cupriolinic blue. After fixation overnight at 4°C, the tissues were rinsed three times in sodium acetate buffer with $MgCl_2$. Small pieces of skin containing either wounded or unwounded areas were obtained, stained with 1% phosphotungstinic acid for 1 hour, and washed. Samples were then dehydrated and embedded in Epon resin (Ted Pella, Inc., Redding, CA). Sections that were approximately 60 to 70 nm thick were cut on a Reichert-Jung Ultracut E ultramicrotome (Reichert-Jung, Austria) and picked up on formvar-coated copper grids. The sections were stained with uranyl acetate and Reynolds lead citrate and examined on a JEOL 100CX electron microscope at 80 kV at ×72,000 magnification.[25] Eight radiographs were taken per sample and the radiographs were scanned using Epson 2100 at 300 dots per inch (Figure 1D). Approximately 15,000 fibers were manually measured using the ImagePro software (Media Cybernetics, Bethesda, MD).

Statistical Analysis

The results were graphically depicted as mean ± SD. Two-tailed *t* test and one-way analysis of variance were performed (SPSS 11.0 for Windows, SPSS, Chicago, IL) to detect statistically significant differences. *P* value <0.05 was considered significant.

Results

Dermal Thickness

No significant difference was found in the dermal thickness between $FMOD^{-/-}$ animals when compared with sex- and age-matched WT controls (Figure 2A). However, dermal thickness was significantly larger in younger male mice (3 to 4 months) compared with older male mice (5 to 6 months) (Figure 2B). H&E histology also showed significantly larger dermal thickness in male mice compared with age-matched female mice (Figure 2C). Lastly, a significant reduction in dermal thickness was observed in the analyzed scars with increasing scar age (Figure 2D). We also observed that the most reliable thickness measurements with lowest variance were from T1 and T4 (Figure 1, A and B), which were equidistant, farther away from the wound site, and spanned all of the way from the epidermal-dermal junction down to the panniculus carnosus (variance data not shown).

Scar Index Analysis

H&E histology of 14-day postoperative wounds of 5- to 6-month-old $FMOD^{-/-}$ animals exhibited a much larger area of fibrosis compared with age-matched WT controls (Figure 3, A–H). Furthermore, as expected, the fibrotic areas in both genotypes were completely devoid of adnexal structures (Figure 3, A–H). Quantitative analysis of scar size showed that $FMOD^{-/-}$ animal scars were on average 143% larger than those of WT animals (Figure 3I). This result was confirmed by Masson's trichrome

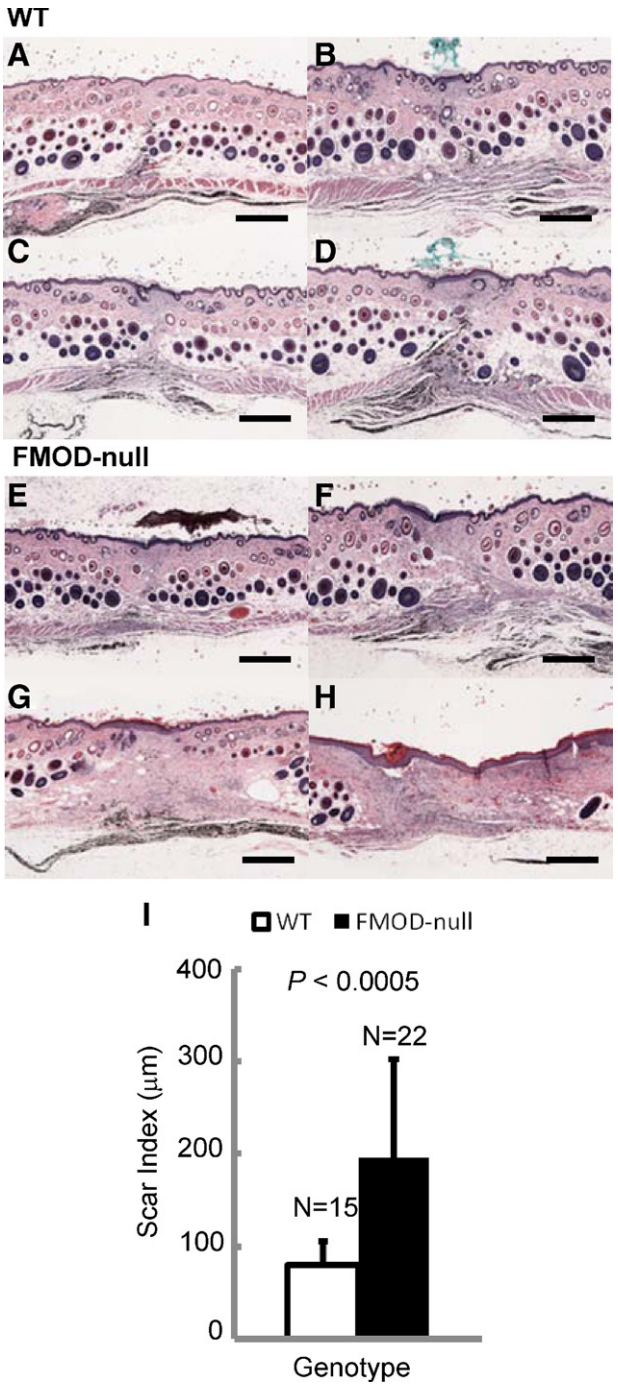

Figure 3. H&E analysis of cutaneous scar tissue from FMOD-null mice reveals significantly increased scarring. Light microscopy of postoperative day 14 skin wounds in 5- to 6-month-old WT (**A–D**) and FMOD-null (**E–H**) mice. Representative scars in descending order from smallest (**A** and **E**) to largest (**D** and **H**). Quantitative Scar Index analysis revealed that FMOD-null scars were on average 143% larger than WT scars (**I**). Scale bars = 500 μm.

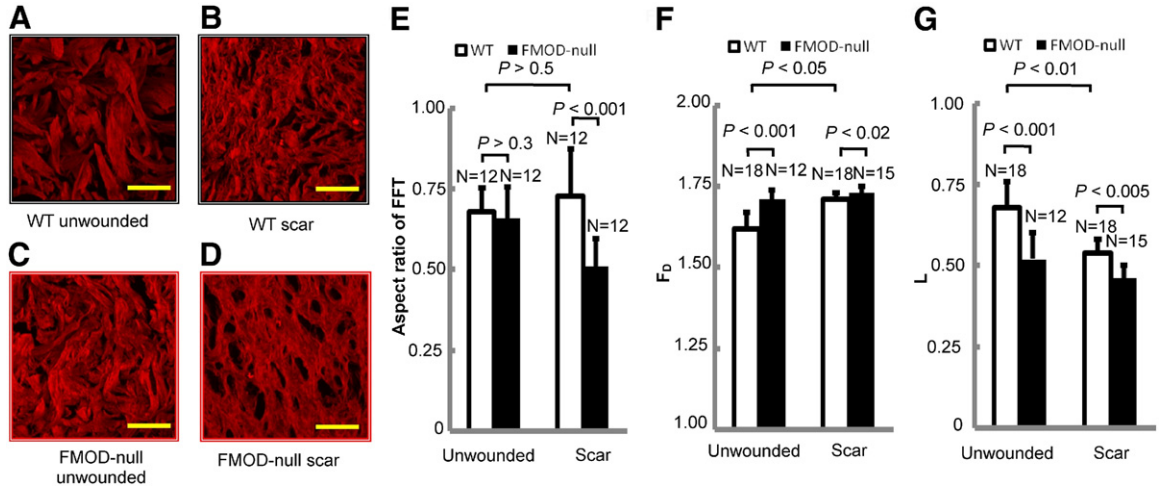

Figure 4. Confocal microscopy of unwounded and wounded skin from FMOD-null mice reveals significant losses in architectural complexity. Confocal microscopy of unwounded dermis (**A** and **C**) and wounded dermis (postoperative day 14) (**B** and **D**) in 5- to 6-month-old WT (**A** and **B**) and FMOD-null (**C** and **D**) mice. Fourier transform analysis (**E**) failed to distinguish the difference between unwounded WT and FMOD-null skin and between unwounded and wounded skin of WT mice. Note how the loss of a more random, "basket-weave–like" pattern in FMOD$^{-/-}$ animals (**C** and **D**) corresponded to an increased structural density that is reflected by increased F_D (**F**) and a reduced structural heterogeneity that is reflected by decreased L (**G**). Scale bars = 25 μm.

staining and picro Sirius red staining (see Supplemental Figure S1 at *http://ajp.amjpathol.org*).

Confocal Laser Scanning Microscope Images of Collagen Bundles

Confocal laser scanning microscope (CLSM) images of dermal collagen from unwounded skin of 5- to 6-month-old FMOD$^{-/-}$ animals showed a significant change in architectural organization (higher collagen density and smaller collagen bundle size) compared with age-matched WT controls (Figure 4, A and C). In addition, the typical basket-weave–like pattern of dermal collagen bundles in unwounded skin (Figure 4, A and C) was tremendously diminished in the scar tissue of both WT and FMOD$^{-/-}$ animals (Figure 4, B and D).

Image-Pattern Analysis with Fourier Transform of CLSM Images

Fourier transform analysis of CLSM images at high magnification (1000×; Figure 4, A–D) showed a statistically significant difference between WT and FMOD$^{-/-}$ scar. However, it failed to show a statistically significant difference between WT and FMOD$^{-/-}$ unwounded animals and between scar and unwounded WT animals (Figure 4E).

Fractal Dimension and Lacunarity Analysis of CLSM Images

FMOD$^{-/-}$ animals had significantly larger F_D value than did the age-matched WT animals, indicating increased collagen density (Figure 4F). In addition, FMOD$^{-/-}$ animals also had a significantly lower L value than did the age-matched WT animals (Figure 4G), which indicates a loss of structural complexity. Meanwhile, scar tissue of FMOD$^{-/-}$ and WT animals had higher F_D value and lower L value compared with unwounded skin.

TEM

TEM of dermal collagen from unwounded skin of 5- to 6-month-old FMOD$^{-/-}$ animals showed marked ultrastructural abnormalities. First, collagen fibrils exhibited a great variability in shape and size (Figure 5E); in cross-section, individual fibrils had irregular outlines compared with the circular and uniform outline of controls (Figure 5B). Second, multiple giant fibrils were identified with very large diameters up to 320 nm (Figure 5E, asterisk) and showed scalloped edges or focal lateral fusion with thinner fibrils (Figure 5E, arrow). In addition, the collagen fibrils were packed in a less orderly way, as evidenced by the increase in negative space between the fibrils of FMOD$^{-/-}$ animals compared with age-matched WT controls (Figure 5D, star). The fibrils in unwounded skin of FMOD$^{-/-}$ animals were significantly larger than in unwounded skin of WT animals (Figure 5, C and F). Furthermore, FMOD$^{-/-}$ animals exhibited a wider range of fibril diameter, ranging from 90 to 330 nm (Figure 5F), compared with that of WT animals, ranging from 70 to 230 nm (Figure 5C).

Ultrastructural analysis of dermal collagen from scar tissue of 5- to 6-month-old FMOD$^{-/-}$ animals showed similar structural changes. The fibrils in scar tissue were irregular in shape and size and were packed in a less orderly way in FMOD$^{-/-}$ animals (Figure 5K). In comparison, the fibrils from the scar tissue of the age-matched WT animals had a normal appearance, with round and smooth fibrils that were packed in a more orderly way (Figure 5H). The fibrils in scar tissue of FMOD$^{-/-}$ animals were significantly larger than in the WT animals (Figure 5, I and L). Similar to FMOD$^{-/-}$ unwounded tissue, the scar tissue of FMOD$^{-/-}$ animals exhibited a wider range of fibril diameter, ranging from 50 to 310 nm (Figure 5L), compared with the WT animals' extremely narrow scar tissue range of 30 to 150 nm (Figure 5I). Overall, fibrils from scar tissue of WT and FMOD$^{-/-}$ animals were approximately half the size of fibrils of the corresponding unwounded tissue.

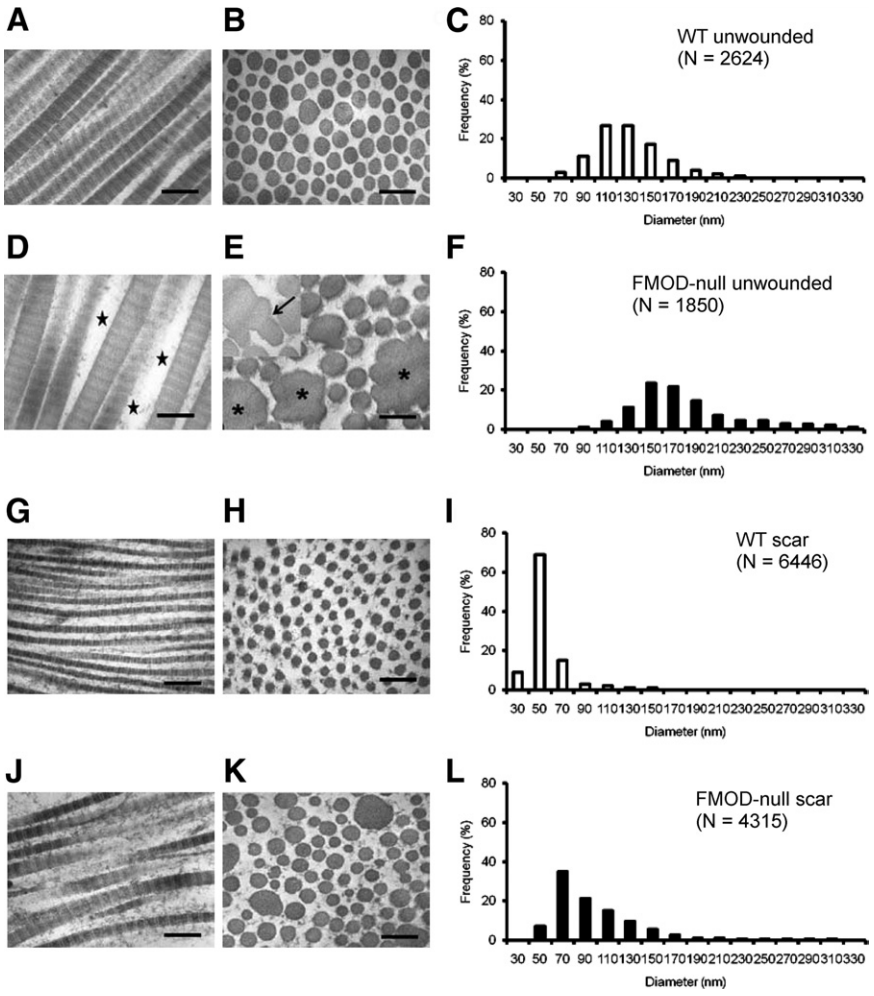

Figure 5. Ultrastructural analysis of unwounded and wounded skin from FMOD-null mice reveals marked abnormalities in collagen fibrillogenesis. TEM of unwounded dermis (**A**, **B**, **D,** and **E**) and wounded dermis (postoperative day 14) (**G**, **H**, **J**, and **K**) of 5- to 6-month-old WT mice (**A**, **B**, **G**, and **H**) and FMOD-null mice (**D**, **E**, **J**, and **K**) and corresponding frequency distributions (**C**, **F**, **I**, and **L**). Longitudinal fibrils illustrating typical banding periodicity of 67 nm in type I collagen (**A**, **D**, **G**, and **J**) and the cross-sectional fibril profile (**B**, **E**, **H**, and **K**) showed the overall shape and size of the fibrils. Compared with unwounded skin (**A–F**), wounded skin (**G–L**) contained much smaller fibrils in all animals. Note the variability in the shape (**E** and **K**) and size (**F** and **L**) of FMOD-null fibrils, the presence of giant fibrils with irregular borders (**E**, **asterisks**), and scalloped edges representing focal lateral fusion with thinner fibrils (**E**, **arrow**). Note also the increased negative space between the fibrils in FMOD-null animals (**D**, **star**). In contrast, fibrils from WT animals (**A**, **B**, **G**, and **H**) showed a more orderly spacing with circular, uniformly shaped fibrils. Scale bars = 200 nm.

In addition, the decrease in fibril size is greater in FMOD$^{-/-}$ animals compared with WT animals; WT scar tissue fibrils are 43% smaller than in WT unwounded animals, while FMOD$^{-/-}$ scar tissue fibrils are 60% smaller than in FMOD$^{-/-}$ unwounded animals.

Discussion

To our knowledge this is the first study that has applied F_D and *L* concepts for quantitative morphometric analysis of dermal collagen architecture. This method has proved to be an easy, sensitive, reproducible, and objective technique that provides proper quantification of not only scar but also unwounded dermis collagen morphology. Use of F_D and *L* analysis is much more objective when compared with using light microscopy with polarized light, because observer bias is avoided. Because confocal microscopy takes advantage of the fluorescence properties of collagen, it provides higher-resolution images of the dermal structure with better rejection of out-of-focus information than does conventional light microscopy.[26] Although F_D and *L* analysis was only performed on confocal microscopy images in this study, this method also can be applied to images obtained from fluorescence microscopy.

In this study, F_D and *L* analysis was able to discern significant differences in architectural collagen organization between adult WT mice cutaneous scar tissue and unwounded tissue. Collagen bundles in scar tissue exhibited denser (higher F_D) and more homogeneous (lower *L*) architecture compared with the looser, basket-weave–like pattern and randomly organized collagen bundles of unwounded tissue. This increase in density and loss of heterogeneity was even more evident in the scar tissue of FMOD$^{-/-}$ mice. Moreover, significant differences in the dermal architectural organization were also observed between unwounded skin from WT and FMOD$^{-/-}$ animals. These data demonstrate the utility and discriminatory capability of F_D and *L* analysis to further define and quantify collagen morphology in unwounded, wounded, and genotypically different skin specimens.

Furthermore, we compared F_D and *L* analysis with Fourier transform analysis because the latter has been demonstrated to be the superior method in analyzing collagen morphology.[3,4] Fourier transform analysis failed to show a statistically significant difference between WT and FMOD$^{-/-}$ unwounded dermis and between scar tissue and unwounded tissue of WT animals. A possible explanation for this observation may be the fact that we

used higher-magnification images of the collagen bundles compared with previous studies using Fourier analysis (1000× objective versus 5×).[3,5,12] Unlike Fourier transform analysis, fractal calculations change as the analyzed pixel size in the image gets smaller. Therefore as the image resolution is increased, more accurate F_D and *L* values are obtained.[13] In contrast, Fourier transform analysis is very sensitive in determining average collagen bundle orientation in a defined region only. At low magnification many bundles are present in the image and the average orientation and complexity is picked up easily. However, as the magnification is increased, the image contains only a few bundles and consequently the average orientation calculations become less accurate, while F_D and *L* analysis demonstrated superiority at this scale in this study.

To determine whether differences in F_D and *L* data on collagen bundle architecture are associated with any differences in collagen ultrastructure, we evaluated the ultrastructural morphology of 15,000 collagen fibrils. Collagen fibrils in WT adult mouse scars after 14 days of healing were 57% of the diameter of WT unwounded tissue. In comparison, the collagen fibrils of 14-day scars of $FMOD^{-/-}$ mice were only 40% of the fibril diameter of $FMOD^{-/-}$ unwounded tissue. The $FMOD^{-/-}$ animals also exhibited a wider range of fibril diameter and were less orderly packed. $FMOD^{-/-}$ mice also showed major abnormalities in collagen fibril structure. A striking difference was the presence of many giant fibrils with diameters reaching 320 nm. These fibrils had scalloped edges and demonstrated focal lateral fusion with smaller fibrils. It is likely that this continuous state of fusion contributes to the variability in the shape and size of the fibrils seen in the $FMOD^{-/-}$ animals. In contrast, focal lateral fusion was not observed in WT animal fibrils, and the fibrils were uniform in size and shape. As a result of this fusion process, unwounded $FMOD^{-/-}$ mouse fibril diameters were on average 53% larger than those of control animals. The $FMOD^{-/-}$ mouse fibrils also were packed in a less orderly way as evidenced by the increased interfibrillar space between them. It is likely that the variability in the morphology of the fibrils caused by this continuous state of fusion interferes with the packing of collagen bundles. Similar observations have been seen in animals deficient in decorin[27] and lumican,[28] indicating that these small leucine-rich proteoglycans are able to bind to the surface of type I collagen at various sites and prevent the lateral fusion of collagen fibrils and hence modulate their size and ability to form organized bundles. Overall, these data demonstrate that phenotypic differences detectable by F_D and *L* analysis are also associated with differences in collagen ultrastructure. For future studies, it would be of interest to examine if F_D and *L* data can be *predictive* of altered collagen ultrastructure.

Additionally, a simple, objective, accurate, and reproducible approach to quantifying scar size also was established in this study. Previous studies have used only the width of the fibrotic area as a measure of scar size and did not delineate the entire scar area.[29,30] By dividing the scar area by the corresponding average scar thickness, our methodology not only measures the entire scar area but is also able to account for variability in skin thickness. Using this approach, we demonstrated that in addition to anatomic regional differences, various other factors such as age, sex, and scar age could influence dermal thickness. Therefore in determining scar size it is crucial to standardize for dermal thickness because a thicker dermis will result in thicker scars with larger fibrotic areas.

In summary, we have demonstrated a new objective and quantitative approach to analysis of scar collagen morphology and scar size. Our data illustrate that F_D and *L* analysis is a sensitive, reproducible, and objective technique that can be used to provide superior quantification of scar quality. This method is also more sensitive and less labor intensive compared with other objective techniques available, such as X-ray diffraction, laser scattering, and Fourier transform analysis. Because F_D and *L* analysis can be used to investigate dermal architecture, this method has wide application in wound healing research. It can analyze and "fingerprint" any fibrotic tissue and be applied to evaluation of fibrotic disorders such as keloids, hypertrophic scars, lichen sclerosis, and scleroderma. Based on our ability to detect significant differences in unwounded skin from WT and $FMOD^{-/-}$ mice, F_D and *L* analysis also may find clinical usefulness in analysis of disorders with abnormal collagen structure, such as Ehlers-Danlos syndrome, Marfan syndrome, and osteogenesis imperfecta. In addition, we were able to demonstrate that quantitative F_D and *L* differences between WT and $FMOD^{-/-}$ mice also correlated with altered collagen ultrastructure, directly supporting FMOD's role in binding collagen and regulating fibrillogenesis and influencing the overall structural size and architecture of scar tissue.

Acknowledgments

We thank Dr. Grace Xinlian Chang (University of California at Los Angeles) for her assistance with animal surgeries and Dr. Marianne Cilluffo (Microscopic Techniques Laboratory). CLSM was performed at the Center for NanoScience Institute Advanced Light Microscopy/Spectroscopy Shared Resource Facility at the University of California at Los Angeles.

References

1. Gibson T: The physical properties of skin. Edited by J Converse. Philadelphia, WB Saunders, 1990, pp 207–220
2. Peacock E: Contraction. Edited by E Peacock. Philadelphia, WB Saunders, 1984, pp 38–90
3. van Zuijlen PP, de Vries HJ, Lamme EN, Coppens JE, van Marle J, Kreis RW, Middelkoop E: Morphometry of dermal collagen orientation by Fourier analysis is superior to multi-observer assessment. J Pathol 2002, 198:284–291
4. Verhaegen PD, Res EM, van Engelen A, Middelkoop E, van Zuijlen PP. A reliable, non-invasive measurement tool for anisotropy in normal skin and scar tissue. Skin Res Technol 2010, 16:325–331
5. van Zuijlen PP, Ruurda JJ, van Veen HA, van Marle J, van Trier AJ, Groenevelt F, Kreis RW, Middelkoop E: Collagen morphology in hu-

man skin and scar tissue: no adaptations in response to mechanical loading at joints. Burns 2003, 29:423–431
6. Wolman M, Gillman T: A polarized light study of collagen in dermal wound healing. Br J Exp Pathol 1972, 53:85–89
7. Wolman M, Kasten FH: Polarized light microscopy in the study of the molecular structure of collagen and reticulin. Histochemistry 1986, 85:41–49
8. Brodsky B, Ramshaw JA: Collagen organization in an oriented fibrous capsule. Int J Biol Macromol 1994, 16:27–30
9. Purslow PP, Wess TJ, Hukins DW: Collagen orientation and molecular spacing during creep and stress-relaxation in soft connective tissues. J Exp Biol 1998, 201:135–142
10. Ferdman AG, Yannas IV: Scattering of light from histologic sections: a new method for the analysis of connective tissue. J Invest Dermatol 1993, 100:710–716
11. Bowes LE, Jimenez MC, Hiester ED, Sacks MS, Brahmatewari J, Mertz P, Eaglstein WH: Collagen fiber orientation as quantified by small angle light scattering in wounds treated with transforming growth factor-beta2 and its neutralizing antibody. Wound Repair Regeneration 1999, 7:179–186
12. de Vries HJ, Enomoto DN, van Marle J, van Zuijlen PP, Mekkes JR, Bos JD: Dermal organization in scleroderma: the fast Fourier transform and the laser scatter method objectify fibrosis in nonlesional as well as lesional skin. Lab Invest 2000, 80:1281–1289
13. Smith TG Jr., Lange GD, Marks WB: Fractal methods and results in cellular morphology–dimensions, lacunarity and multifractals. J Neurosci Methods 1996, 69:123–136
14. Mandelbrot BB: The fractal geometry of nature. New York, W.H. Freeman & Co., 1983, pp 14–19, 310–318
15. Eblen-Zajjur A, Salas R, Vanegas H: Fractal analysis of spinal dorsal horn neuron discharges by means of sequential fractal dimension D. Comput Biol Med 1996, 26:87–95
16. Tinajero JP, Robledo RF, Lantz RC, Sobonya RE, Quan SF, Lemen RJ, Tollinger BJ, Witten ML: Fractal analysis of lung alveoli during the acute phase vs. repair phase of an adenoviral infection in canines. Res Commun Mol Pathol Pharmacol 1997, 95:275–285
17. Guidolin D, Vacca A, Nussdorfer GG, Ribatti D: A new image analysis method based on topological and fractal parameters to evaluate the angiostatic activity of docetaxel by using the Matrigel assay in vitro. Microvasc Res 2004, 67:117–124
18. Oldberg A, Antonsson P, Lindblom K, Heinegard D: A collagen-binding 59-kd protein (fibromodulin) is structurally related to the small interstitial proteoglycans PG-S1 and PG-S2 (decorin). EMBO J 1989, 8:2601–2604
19. Vogel KG, Trotter JA: The effect of proteoglycans on the morphology of collagen fibrils formed in vitro. Coll Relat Res 1987, 7:105–114
20. Garg AK, Berg RA, Silver FH, Garg HG: Effect of proteoglycans on type I collagen fibre formation. Biomaterials 1989, 10:413–419
21. Svensson L, Narlid I, Oldberg A: Fibromodulin and lumican bind to the same region on collagen type I fibrils. FEBS Lett 2000, 470:178–182
22. Hedlund H, Mengarelli-Widholm S, Heinegard D, Reinholt FP, Svensson O: Fibromodulin distribution and association with collagen. Matrix Biol 1994, 14:227–232
23. Font B, Eichenberger D, Goldschmidt D, Boutillon MM, Hulmes DJ: Structural requirements for fibromodulin binding to collagen and the control of type I collagen fibrillogenesis–critical roles for disulphide bonding and the C-terminal region. Eur J Biochem 1998, 254:580–587
24. Soo C, Beanes SR, Hu FY, Zhang X, Dang C, Chang G, Wang Y, Nishimura I, Freymiller E, Longaker MT, Lorenz HP, Ting K: Ontogenetic transition in fetal wound transforming growth factor-beta regulation correlates with collagen organization. Am J Pathol 2003, 163: 2459–2476
25. Scott JE, Orford CR: Dermatan sulphate-rich proteoglycan associates with rat tail-tendon collagen at the d band in the gap region. Biochem J 1981, 197:213–216
26. Dolber PC, Spach MS: Conventional and confocal fluorescence microscopy of collagen fibers in the heart. J Histochem Cytochem 1993, 41:465–469
27. Danielson KG, Baribault H, Holmes DF, Graham H, Kadler KE, Iozzo RV: Targeted disruption of decorin leads to abnormal collagen fibril morphology and skin fragility. J Cell Biol 1997, 136:729–743
28. Chakravarti S, Magnuson T, Lass JH, Jepsen KJ, LaMantia C, Carroll H: Lumican regulates collagen fibril assembly: skin fragility and corneal opacity in the absence of lumican. J Cell Biol 1998, 141:1277–1286
29. Cheon SS, Wei Q, Gurung A, Youn A, Bright T, Poon R, Whetstone H, Guha A, Alman BA: Beta-catenin regulates wound size and mediates the effect of TGF-beta in cutaneous healing. FASEB J 2006, 20:692–701
30. Stoff A, Rivera AA, Mathis JM, Moore ST, Banerjee NS, Everts M, Espinosa-de-Los-Monteros A, Novak Z, Vasconez LO, Broker TR, Richter DF, Feldman D, Siegal GP, Stoff-Khalili MA, Curiel DT: Effect of adenoviral mediated overexpression of fibromodulin on human dermal fibroblasts and scar formation in full-thickness incisional wounds, J Mol Med 2007, 85:481–496